

TLDR: Traffic Light Detection using Fourier Domain Adaptation in Hostile WeatheR

Ishaan Gakhar¹, Aryesh Guha^{2,7}, Aryaman Gupta^{3,7}, Amit Agarwal⁴, Durga Toshniwal⁵, Ujjwal Verma^{6,1}

¹Department of Information and Communication Technology, Manipal Institute of Technology, Manipal Academy of Higher Education

²Department of Electrical and Electronics Engineering, Manipal Institute of Technology, Manipal Academy of Higher Education

³Department of Computer Science Engineering, Manipal Institute of Technology, Manipal Academy of Higher Education

⁴Enterprise Analytics & Data Science Artificial Intelligence - Center of Excellence Wells Fargo International Solutions Private Limited

⁵Center For Transportation Systems, Indian Institute of Technology Roorkee

⁶Manipal Institute of Technology Bengaluru, Manipal Academy of Higher Education

⁷These authors contributed equally to this work.

Abstract—The scarcity of comprehensive datasets in the traffic light detection and recognition domain and the poor performance of state-of-the-art models under hostile weather conditions present significant challenges. To address these issues, this paper proposes a novel approach by merging two widely used datasets, LISA and S²TLD. The merged dataset is further processed to tackle class imbalance, a common problem in this domain. This merged dataset becomes our source domain. Synthetic rain and fog are added to the dataset to create our target domain. We employ Fourier Domain Adaptation (FDA) to create a final dataset with a minimized domain gap between the two datasets, helping the model trained on this final dataset adapt to rainy and foggy weather conditions. Additionally, we explore Semi-Supervised Learning (SSL) techniques to leverage the available data more effectively. Experimental results demonstrate that models trained on FDA-augmented images outperform those trained without FDA across confidence-dependent and independent metrics, like mAP50, mAP50-95, Precision, and Recall. The best-performing model, YOLOv8, achieved a Precision increase of 5.1860%, Recall increase of 14.8009%, mAP50 increase of 9.5074%, and mAP50-95 increase of 19.5035%. On average, percentage increases of 7.6892% in Precision, 19.9069% in Recall, 15.8506% in mAP50, and 23.8099% in mAP50-95 were observed across all models, highlighting the effectiveness of FDA in mitigating the impact of adverse weather conditions on model performance. These improvements pave the way for real-world applications where reliable performance in challenging environmental conditions is critical.

Impact Statement—This research addresses a critical challenge in autonomous driving systems—poor performance in adverse weather conditions—by introducing a novel method using Fourier Domain Adaptation (FDA). The FDA-enhanced models significantly improve the detection of traffic lights in rain and fog, which has broad implications for the safety and effectiveness of advanced driving assistance systems (ADAS). These advancements contribute to the reliability of AI in real-world scenarios, reducing the risk of accidents. Beyond autonomous driving, the findings benefit industries like drone navigation and surveillance, enhancing performance under challenging weather. Ultimately, this research strengthens AI's ability to operate safely and effectively, advancing the field of AI while addressing pressing

societal safety concerns.

Index Terms—Adverse Weather, Autonomous Driving, Detection in Adverse Weather, Fourier Domain Adaptation, Object Detection, Semi-supervised Learning, Synthetic Dataset, Traffic Light Detection

I. INTRODUCTION

Environmental perception, along with behaviour decision and motion control, is an essential task in the domain of autonomous driving. With artificial intelligence and computer vision techniques playing integral roles in autonomous driving, object detection plays a crucial role in understanding surrounding environmental scenarios [1], [2]. Adverse weather conditions compromise sensor accuracy and real-time performance, resulting in image degradation issues. This ultimately affects the object detection performance of autonomous vehicles [3], [4].

Detecting and recognizing traffic lights is important for ensuring safety in the field of autonomous driving. Vision-based traffic light detection and recognition in traffic scenes is still a challenge [5], [6] to be successfully overcome by the autonomous driving industry, especially when there are disturbances due to weather conditions that contribute to the degradation in the performance of object detection models. State-of-the-art (SOTA) object detection algorithms, like YOLOv5 [7], YOLOv6 [8], YOLOv8 [9] and YOLOv10 [10], perform well in clear weather conditions. However, when used in detrimental weather conditions, such as environments with rain or fog, a significant deterioration in their performance is observed, as discussed later in our work.

Unsupervised Domain Adaptation (UDA) is a form of transfer learning that involves adapting a model trained on one domain that has an abundance of annotations (source domain) to demonstrate results in a related yet distinct domain (target domain) characterized by a different data distribution

that lacks annotations. Training the model solely within the source domain fails to produce satisfactory outcomes owing to the occurrence of covariate shift as mentioned in [11]. The primary objective of domain adaptation techniques is to facilitate knowledge transfer from a well-labelled source domain to a target domain that lacks labels. This process is essential, as minor alterations in low-level statistics notably impact the model's effectiveness. This is particularly relevant for leveraging existing datasets with annotations to enhance performance on related tasks that lack such annotations, like Advanced Driver Assistance Systems (ADAS), security and surveillance systems, etc. Domain adaptation thus plays a pivotal role in addressing the challenge of data scarcity in supervised learning scenarios by bridging the discrepancy between different but related domains.

In our work, we combine widely used datasets LISA [12] and SJTU: Small Traffic Light Dataset (S²TLD) [13] while using various augmentations to address the class imbalance against images containing yellow traffic lights to form our source domain. Leveraging pre-existing techniques for fog addition [14] and rain addition¹, we create a new dataset of rainy and foggy images using the images from our source dataset. This dataset serves as our target domain. We use Fourier Domain Adaptation (FDA) [11], where the Fast Fourier Transform (FFT) of each input image (clear weather) is computed, and the low-level frequencies of the target image (rainy or foggy) replace the low-level frequencies of the source image before the images are reconstituted for training using Inverse FFT (iFFT).

A particular range of beta was chosen based on [11], and various values taken from that range were tested using various objection detection models. This leads to the model learning domain invariant features, i.e., traffic lights, which allows it to perform traffic light detection better than a model that was trained on a dataset with clear weather conditions in a rainy/foggy environment as observed in Fig 1 and Fig 6. The source dataset was benchmarked using various state-of-the-art methods, and their performance was qualitatively and quantitatively evaluated across different metrics (confidence dependent and independent). To address the lack of traffic light detection datasets, we used semi-supervised learning (SSL). YOLOv6 was first trained on 50% of the training data, generating pseudo-labels for the other 50%. These pseudo-labels were combined with the original labels to create a new training set. Several models were then trained on this augmented dataset to show the effectiveness of SSL. The results from inference on the target domain dataset are discussed in the next section. The contributions of our work are:

- Combining widely used datasets and addressing class imbalance to synthetically generate realistic rainy and foggy images by means of effective pre-existing methods.
- Proposing and demonstrating the efficacy of Fourier Domain Adaptation for Traffic Light detection in adverse weather conditions.
- Implementing Semi-Supervised Learning in the realm of Traffic Light Detection as a potential solution to the lack

of datasets in the domain.

The paper is structured as follows, Section II discusses prior works adjacent to the domains relevant to this paper, Section III details the proposed methodology employed for the aforementioned problem statement of traffic light detection in hostile weather conditions. Later, section IV describes the experimental setup to justify the choice of hyperparameters. Further, in Section V, we discuss the results of our methodology by benchmarking with various unique SOTA models and explore the effect of FDA and SSL through qualitative and quantitative evaluation.

II. RELATED WORKS

A. Object Detection

In recent years, significant advancements have been made in object detection, driven by the development of deep learning-based techniques. One of the most influential works is the YOLO (You Only Look Once) series, introduced by Redmon et al., which revolutionized object detection by achieving real-time performance while maintaining high accuracy. YOLOv3 [15] and its successors, YOLOv5 [7] and YOLOv8 [9], have further improved detection capabilities by incorporating advanced features and optimization techniques. Additionally, Mask R-CNN by He et al. [16] extended Faster R-CNN by adding a branch for predicting segmentation masks, thereby providing a unified approach for object detection and instance segmentation. A novel object detection model that leverages transformers instead of traditional CNNs was introduced in [17]. It simplifies the object detection pipeline by directly predicting bounding boxes and class labels from image pixels, eliminating the need for anchor boxes and non-maximum suppression. The model achieves competitive performance on standard benchmarks while offering a more streamlined approach to object detection. These pioneering works have laid the foundation for numerous subsequent studies, contributing to the rapid evolution and diversification of object detection methodologies.

B. Detection in Unfavourable Weather Conditions

Object detection in bad weather conditions has been a topic of recent interest to improve the efficacy of autonomous vehicles and surveillance systems. The use of YOLOv5 for real-time identification of cars, traffic lights, and pedestrians in various weather conditions, including challenging scenarios like rain and fog, is explored in [18]. A novel approach has been used in [19] combining visible and infrared image features using a CNN. By fusing these complementary features, the method enhances the accuracy of detection in low-visibility conditions, improving system robustness in challenging environments. A network based on the joint optimal learning of an image-defogging module (IDOD) and YOLOv7 detection modules is proposed in [3]. This approach is designed for low-light foggy images, where the SAIP module's parameters are predicted by a separate CNN network, and the AOD module performs defogging by optimizing the atmospheric scattering model..

¹<https://github.com/ShenZheng2000/Rain-Generation-Python>

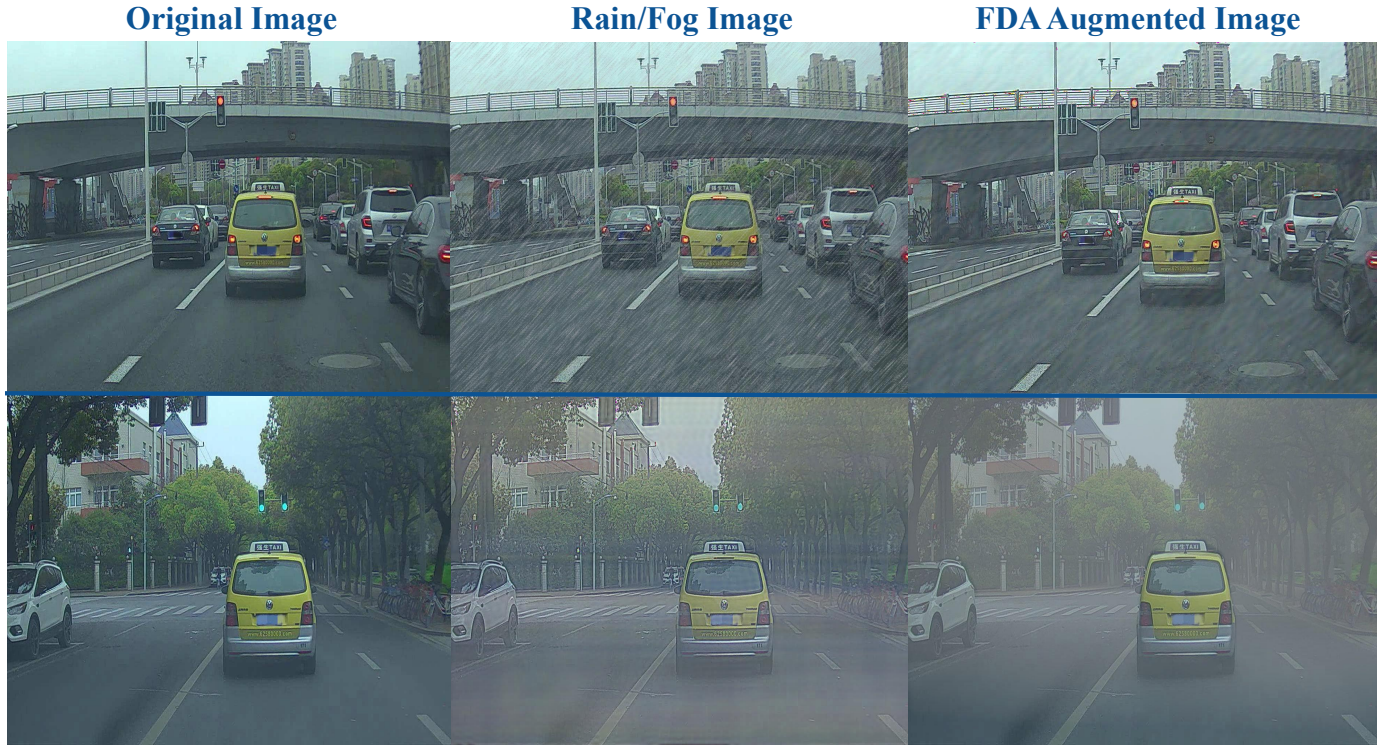


Fig. 1. The first row of images has rain added to them, and the second row has fog added to them. As evident, applying FDA to the images increases visibility and ability to detect.

C. Traffic Light Detection

Detection and recognition of traffic lights are crucial components for the safety and efficiency of autonomous vehicles and intelligent transportation systems. In [20], the authors first passed the images through a deep neural objection detection architecture to get traffic light candidates and then used a reward-based system where each detected traffic light earns rewards with respect to features extracted from both spatial and temporal domains to reduce false positives. One drawback noted was that the classifier performed poorly for yellow lights, likely due to fewer training examples for them. In order to detect traffic lights at night and at a distance, the paper by Phuc et al. [21] used an approach combining the benefits of hand-crafted features and deep learning techniques. However, this method fails to detect traffic lights in complex regions with many traffic light-like objects. An improved YOLOv4 with a lightweight ShuffleNetv2 backbone, along with an enhanced K-Means clustering algorithm for bounding boxes and a novel CS2A mechanism, was introduced by [22] for traffic light recognition on mobile devices. These updates, combined with data augmentation techniques, improve recognition accuracy, reduce model size, and enhance detection speed and small target recognition. At the same time, though, the overall mAP is limited due to a small dataset, and the model cannot generalize very well due to the poor fitting ability of YOLOv4. [23] was introduced to enhance traffic light detectors in autonomous driving. It uses visual analytics and semantic representation learning with minimal human input to identify robustness issues and summarize detector performance. However, the

current method focuses primarily on object semantics and does not address the broader context of driving scenes. Future work could extend this approach by incorporating additional representation learning components to parse driving scene semantics, providing a more comprehensive understanding of detectors in various contexts.

D. Fourier Domain Adaptation (FDA) for Classification

Domain adaptation is a crucial technique in computer vision, designed to bridge the gap between source and target domains with different distributions. Traditional methods, such as those developed by Tzeng et al. [24] and Long et al. [25], have significantly advanced the field by focusing on feature alignment and adversarial training. An extension of domain adaptation is Fourier Domain Adaptation (FDA), which aligns the spectral properties of images through the Fourier transform. The pioneering work by Yang and Soatto [26] introduced this approach, demonstrating its effectiveness in improving semantic segmentation across domains by transferring low-frequency components. This method has been further explored in various applications; for example, in [27], the authors have used the concept of swapping the low-frequency part of the source and target domains used in FDA using the concept of FPS or farthest point sampling to ensure uniform sampling of samples in order to train a model to classify a grape leaf's disease under different environmental conditions.

E. Semi-Supervised Learning for Classification

As mentioned in the introduction, to the best of our knowledge, no datasets for object detection under adverse weather conditions are known to exist at the time of writing this paper. In this context, semi-supervised learning becomes increasingly important as it leverages both labelled and unlabelled data, addressing the challenge of manually annotating large datasets. To address this issue for the more general domain of traffic signs, the authors have used a combination of weakly supervised and semi-supervised learning in order to address the problems of imbalanced data and optimizing pseudo-labels generated on unlabelled data. A ranking-based pseudo-label generation system has been employed in [28], where certain objects are given more importance than others in the object detection system. Improved performance has been observed with semi-supervised learning compared to supervised learning. Real-time driver distraction detection is crucial for developing driver-centered assistance systems. To reduce labelling costs in the work [29], semi-supervised methods using Laplacian support vector machines and semi-supervised extreme learning machines were evaluated. These methods, which classify driver states (attentive vs. distracted) based on eye and head movements, improved detection performance (G-mean) by 0.0245 on average compared to traditional methods. Leveraging unlabelled data from naturalistic driving records, these semi-supervised approaches increase efficiency in model development.

III. METHODOLOGY

In the domain of traffic light detection and recognition, the scarcity of publicly available datasets poses a significant challenge to the development of models as the abundance of data helps models generalize and adapt better to unseen data. To this end, we combine two widely known traffic light detection and recognition datasets, LISA [12] and S²TLD [13]. In the LISA dataset, images not associated with the specified classes—red, green, and yellow—are removed before merging the two datasets. The images in LISA have a resolution of 1280 x 960, and S²TLD has 2 sets of images where one set has a resolution of 1280 x 720 whereas the other set has a resolution of 1920 x 1080.

TABLE I

A BRIEF SUMMARIZATION OF THE INDIVIDUAL DATASETS WE HAVE COMBINED TO CONSOLIDATE A DATASET WHICH WE FURTHER RESIZE AND MANIPULATE TO PERFORM FOURIER ANALYSIS FOR OUR EXPERIMENTS. AS EVIDENT, THERE INNATELY EXISTS A SEVERE CLASS IMBALANCE AGAINST THE 'YELLOW' CLASS.

Dataset	#Images	#Red	#Green	#Yellow
LISA	38323	48.51%	48.60%	2.88%
S ² TLD	5153	73.29%	56.88%	3.41%

All the images are resized to the resolution of 1280 x 1080 using bicubic interpolation, and the labels are adjusted accordingly. As evident in Table I, a class imbalance against the images containing yellow lights is observed in the combined datasets. To address the issue of class imbalance in our dataset, we implemented four image augmentation techniques

using the Albumentations library [30]: horizontal flip, random brightness contrast adjustment, affine transformation, and blur, each with a probability of 50%, as seen in Fig 2 and Table II. For the random brightness contrast adjustment, brightness and contrast limits were set to 0.2 (brightness_limit=0.2, contrast_limit=0.2) to modulate the image brightness and contrast dynamically. The affine transformation encompassed scaling, translation, rotation, and shearing. The affine transformation included a shear range set between 0 and 20 degrees (shear=(0, 20)). The blur augmentation had a blur limit with a kernel size 7 (blur_limit=7).

TABLE II

THE LIST OF AUGMENTATIONS APPLIED TO ADDRESS THE CLASS IMBALANCE AND THE HYPERPARAMETERS EMPLOYED IN THE PROCESS. ALL THESE HYPERPARAMETERS WERE USED WITH A PROBABILITY OF 0.5

Augmentation	Hyperparameters
Horizontal Flip	p=0.5
Random Brightness Contrast	brightness_limit=0.2, contrast_limit=0.2
Affine	shear=(0,20)
Blur	blur_limit=7

Convergence is observed at 13% yellow images, which is selected as our primary source domain dataset. Using established methods for fog [14] and rain addition², we generate rainy and foggy images from our source domain images, creating our target domain dataset. We employ three sets of hyperparameters to introduce varying degrees of fog and rain into our dataset, aiming to identify the most suitable conditions for our purpose. For fog addition, the hyperparameters we tune are λ and Airlight (γ). The amount of fog in an image is determined by λ , while γ controls the brightness of the foggy image. In the case of rain addition, the hyperparameters include noise, rain_len, rain_angle, rain_thickness, and α . Noise determines the density of rain in the image; rain_len specifies the length of each raindrop; rain_angle dictates the angle of the raindrops relative to the vertical axis; rain_thickness defines the thickness of each raindrop; and α sets the opacity of the raindrops. After extensive experimentation, we believe the suitable set of hyperparameters to be $\lambda = 1$, $\gamma = 150$, noise = 500, rain_len = [50,60], rain_angle = [-50,51], rain_thickness = 3, and $\alpha = 0.7$. The choice and effect of the different sets of hyperparameters are shown in Fig. 4 and further explored in the next section.

$$D^s = \{(x_i^s, y_i^s) \sim P(x^s, y^s)\}_{i=1}^{N_s}, \quad x^s \in R^{H \times W \times 3} \quad (1)$$

As mentioned before, we utilize a source dataset D^s , where x^s represents colour images, and y^s denotes the corresponding bounding box labels. Similarly, the target dataset D_t contains target images without ground truth bounding box labels. As evident in Table III, it is observed that an object detection model trained on D^s experiences a performance drop when tested on D_t and that Fourier Domain Adaptation (FDA) minimizes the domain gap between these datasets. By doing so, we can train a model using the ground truth bounding box



Fig. 2. A visualization of the various methods used to augment images. The first image from the left is the unaltered image, the second is horizontally flipped, the third's contrast and brightness have been altered, the fourth has an affine transformation, and the last has been blurred. The hyperparameters for these augmentations have been mentioned in Table III .

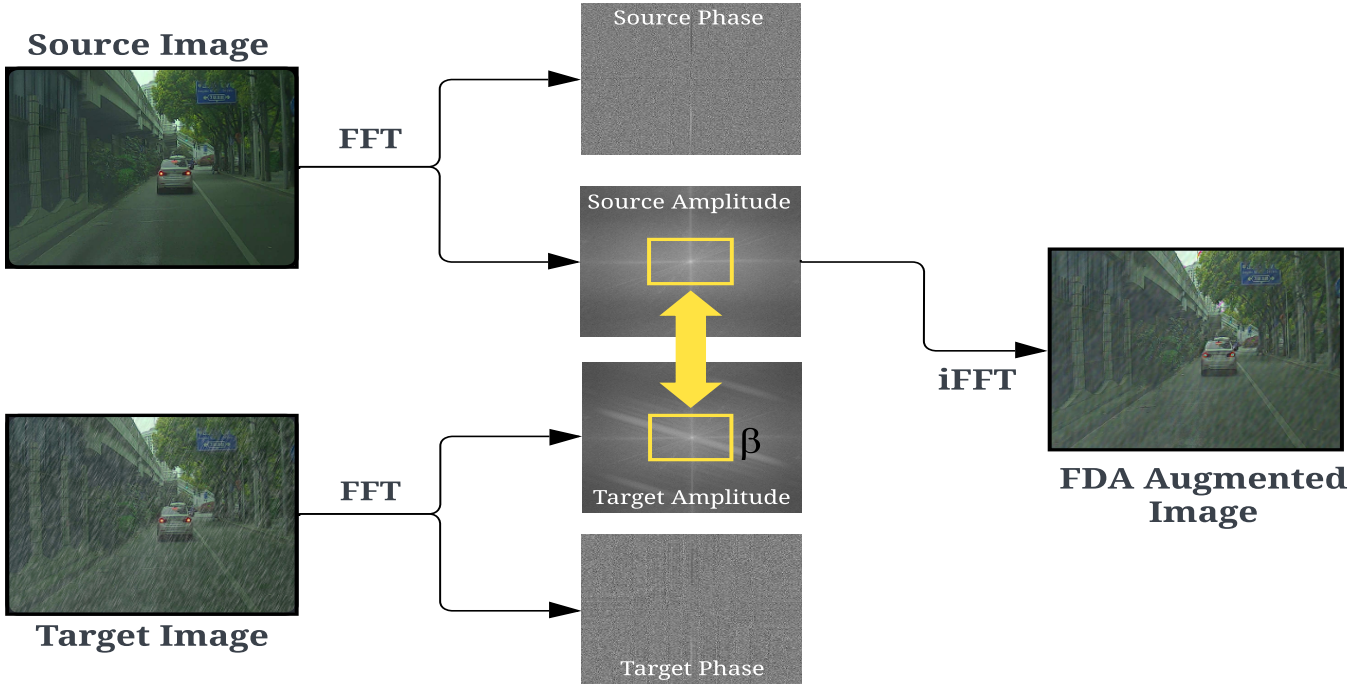


Fig. 3. Shown above is the utilization of a target image to provide the desired style to a source image. The technique achieves this by swapping the low-frequency component of the spectrum of the source image (upper) with that of the target image (lower). The resulting FDA-augmented image exhibits a reduced perceptual domain gap, which helps object detection models adapt better to adverse weather conditions, as mentioned in the benchmarking section. It is important to note that the phase (high-frequency component) and amplitude (low-frequency component) images retain the same resolution as the original images; they are depicted smaller in the diagram solely for visual representation.

labels of the source dataset D^s to enhance performance on the target dataset D^t even though it lacks labels.

The Fourier Transform \mathcal{F} for an image x with a single channel, we get:

$$\mathcal{F}(x)(m, n) = \sum_{h, w} x(h, w) e^{-j2\pi(\frac{h}{H}m + \frac{w}{W}n)}, \quad j^2 = -1 \quad (2)$$

This can be done by implementing (Fast) Fourier Transform (FFT) as in [31]. \mathcal{F}^{-1} represents the inverse Fourier transform, converting spectral signals (phase and amplitude) back into the image space. M_β is a mask whose value is zero except for the center region where $\beta \in (0, 1)$

$$M_\beta(h, w) = 1_{(h, w) \in [-\beta H : \beta H, -\beta W : \beta W]} \quad (3)$$

The centre of the image is considered $(0,0)$. β is not

measured in pixels, therefore the choice of β does not depend on the resolution of the images. Given two randomly sampled images $x^s \sim D^s$ and $x^t \sim D^t$, Fourier Domain Adaptation can be formalized as:

$$x^{s \rightarrow t} = \mathcal{F}^{-1} [M_\beta \circ \mathcal{F}^A(x^t) + (1 - M_\beta) \circ \mathcal{F}^A(x^s), \mathcal{F}^P(x^s)] \quad (4)$$

Where $\mathcal{F}^A, \mathcal{F}^P$: are the amplitude and phase components of the Fourier transform \mathcal{F} of an RGB image.

The low-frequency component of the amplitude of the source image $\mathcal{F}^A(x^s)$ is substituted with that of the target image x^t . The modified spectral representation of x^s , with its phase component retained, is then transformed back into the image $x^{s \rightarrow t}$. This resultant image $x^{s \rightarrow t}$ retains the content of x^s but adopts the appearance of a sample from D^t . Fig. 3 illustrates this process, where the mask M_β has been depicted.

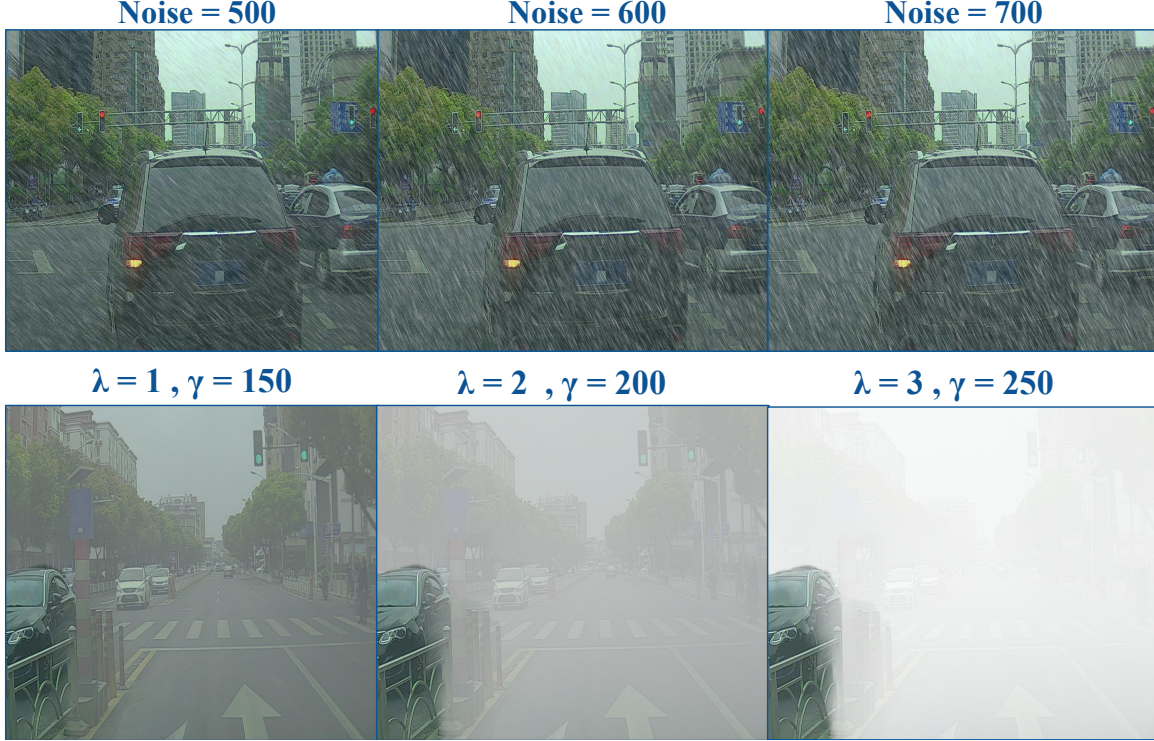


Fig. 4. The first row of images has rain added to them, and the second row has fog added to them. As evident from the images above, the set of hyperparameters, namely Noise=500, $\lambda=1$, and $\gamma=150$, result in a realistic and balanced effect.

We experimented with several values of β , such as 0.1, 0.15, and 0.2. We believe the optimal value of β to be 0.15. The newly adapted source domain dataset $D^{s \rightarrow t}$ was created using this value. The refining effect of FDA can be observed in Fig 1 and Fig 6. The final merged dataset containing the FDA augmented images and the ground truth bounding box labels of source dataset D^s is used to train various state-of-the-art object detection models, such as YOLOv5, YOLOv6, and YOLOv8. As observed in Table IV, subsequent inference on the initial target domain dataset is performed, extensively discussed later.

As mentioned earlier, the domain of traffic light detection and recognition lacks datasets. To address this, we utilize semi-supervised learning (SSL) by training YOLOv6 using 50% of the final dataset's training split. This model generates pseudo-labels for the remaining 50% of the images. These pseudo-labels are combined with the earlier, unchanged labels to create a new set of labels for the train split. YOLOv8 is then trained using the new combined set of labels. Subsequently, inference is performed on the initial target domain dataset, and its results are discussed in the next section.

IV. EXPERIMENTS

A. Dataset Preparation

We have **selectively merged** two widely used datasets - S²TLD and LISA to create a unified dataset for experimentation.

The Shanghai Jiao Tong University (SJTU): Small Traffic Light Dataset (S²TLD) [13] is a newly released dataset designed for traffic light detection and automotive

navigation tasks. It contains 5,786 images, with resolutions of approximately 1920 x 1080 pixels and 1280 x 720 pixels. The dataset includes 14,130 instances categorized into 5 classes: red, yellow, green, off, and wait on. The scenes captured in this dataset cover a diverse range of road conditions, including busy inner-city street scenes, dense stop-and-go traffic, strong changes in illumination and exposure, flickering or fluctuating traffic lights, multiple visible traffic lights, and image parts that can be confused with traffic lights (such as large round tail lights). Our focus within this dataset is on the red, green, and yellow instances under various day and night conditions.

LISA Traffic Light Dataset [12] is a comprehensive resource for traffic light recognition (TLR) tasks used for Autonomous Driving Systems. It consists of images of 14 classes of the resolution 1280 x 960. It contains 43,007 frames and 113,888 annotated traffic lights, out of which we have only used the ones containing red, yellow, and green, captured using a stereo camera mounted on a vehicle. The footage spans both day and night conditions, with varying light and weather conditions.

To address the class imbalance, we experimented with various proportions of yellow traffic light images to identify the optimal percentage for training SOTA models. We trained the models on datasets with various percentages of yellow images, which include 5%, 7%, 9%, 11%, and 13%. Our findings indicate that the dataset comprising 13% yellow images resulted in w , as demonstrated in Fig 5. In our methodology, we defined a source domain D^s with clear images and a target domain D^t with images altered by overlays of rain

and fog. We curated three datasets in the target domain, each with varying levels of rain and fog, as shown in Fig. 4. We concluded through visual inference that the dataset with the aforementioned hyperparameters for rain and fog addition ($\lambda = 1, \gamma = 150, \text{Noise} = 500$) was the most realistic. We applied Fourier Domain Adaptation (FDA) to the source domain images using the target domain images to generate a modified dataset, $D^{s \rightarrow t}$. FDA involved selecting a hyperparameter (β), which determines the size of the spectral neighbourhood swapped between the source and target images. For our experiments, the final dataset was randomly split into 70% for training, 20% for validation, and 10% for testing. The training set consisted of images from $D^{s \rightarrow t}$, the FDA-modified dataset, while the validation and test sets used images from D^t , the target domain with rain and fog effects.

B. Benchmarking

We have tested our approach on several distinct models:

YOLOv5 starts with a strided convolution layer to reduce memory and computational costs, and the SPPF (Spatial Pyramid Pooling Fast) layer accelerates computation by pooling multi-scale features into a fixed-size feature map.

YOLOv6 introduced a new backbone called EfficientRep [32], built on RepVGG [33], which offered greater parallelism than previous YOLO backbones. The network's neck used a PAN (Path Aggregation Network) structure, enhanced with RepBlocks or CSPStackRep Blocks for larger models. This redesigned backbone and neck significantly improved the model's efficiency and adaptability.

YOLOv8 retains a backbone architecture similar to YOLOv5 but introduces significant changes to the CSPLayer, now called the C2f module. This module, which stands for "cross-stage partial bottleneck with two convolutions," effectively merges high-level features with contextual information, resulting in improved detection accuracy.

YOLOv10 introduces a lightweight classification head with depth-wise separable convolutions to reduce computational overhead, Spatial-Channel Decoupled Downsampling to minimize information loss, and Rank-Guided Block Design for

Without FDA With FDA



Fig. 6. Presented here are 2 instances obtained from inferring on YOLOv8m. The first image in each pair is the output of the model trained without FDA, and the second is the output when trained with FDA. Each bounding box has the label (0 implies Red) and the associated confidence score.

optimal parameter use. Accuracy is enhanced through Large-Kernel Convolution for better feature extraction and Partial Self-Attention (PSA) for improved global representation with minimal overhead. It also uses dual label assignments with a consistent matching metric, allowing for rich supervision and efficient deployment without the need for NMS, an integral component of previous YOLO versions.

Each of these YOLO versions differs in their architectural innovations and optimizations, catering to different aspects of object detection challenges. All aforementioned models were trained using the Adam optimizer [34] for 50 epochs on the NVIDIA RTX A6000 GPU with a batch size of 32.

C. Metrics

In our analysis, we employed the metrics mAP50, mAP50-95, Precision, and Recall [35]

The **Mean Average Precision (mAP)** metric provides an overall performance score for object detection models. It is calculated as the mean of the Average Precision (AP) across all classes. The AP for each class is determined by integrating the precision-recall curve, which reflects the model's accuracy at different confidence thresholds. The formula for mAP is:

$$\text{mAP} = \frac{1}{N} \sum_{i=1}^N \text{AP}_i \quad (5)$$

where N is the total number of classes, and AP_i is the Average Precision for the i -th class. For mAP50-95, the AP values are averaged across multiple intersections over union (IoU) [36] thresholds (from 0.50 to 0.95 in 0.05 increments), providing a comprehensive measure of performance across

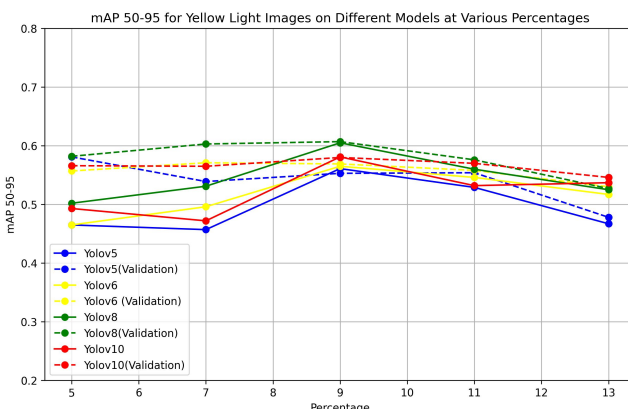


Fig. 5. Benchmarked results of various models on various percentages of yellow lights. It is observed that all models converge at 13%, indicating that the class imbalance is abated.

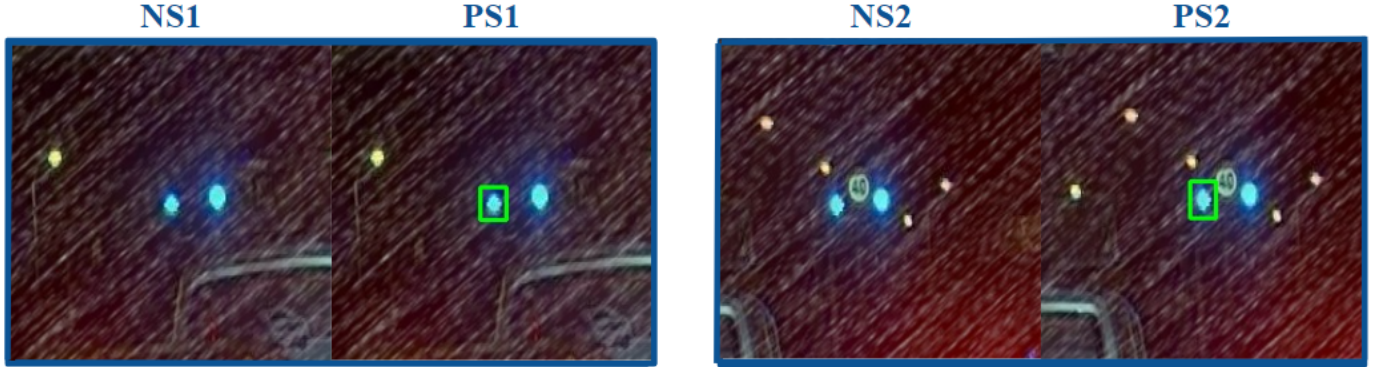


Fig. 7. Comparisons of the instances when trained on the FDA-augmented dataset and trained on the clean dataset. Both instances are derived from YOLOv8. NS refers to negative sample and PS refers to positive sample.

different levels of overlap between predicted and ground truth boxes. mAP50, on the other hand, focuses on a single IoU threshold of 0.50, highlighting the model's ability to detect objects with at least 50% overlap.

Precision is the ratio of true positive detections to all positive detections, indicating how accurate the model's predictions are. It is calculated as:

$$\text{Precision} = \frac{\text{True Positives}}{\text{True Positives} + \text{False Positives}} \quad (6)$$

Recall measures the ratio of true positive detections to all actual objects, demonstrating the model's ability to identify relevant objects. It is defined by:

$$\text{Recall} = \frac{\text{True Positives}}{\text{True Positives} + \text{False Negatives}} \quad (7)$$

It must also be noted that mAP depends on confidence, whereas Precision and Recall are independent. Together, these metrics provide a comprehensive evaluation of the model's performance, particularly in detecting and localizing objects in applications like autonomous driving, surveillance, and monitoring systems.

V. RESULTS

As evident in Table IV, there is a consistent improvement in performance metrics such as precision, recall, mAP50, and mAP50-95 with the increase in β . Benchmarking $D^{s \rightarrow t}$ using the labels of only the source domain indicates best performance at $\beta=0.15$, with YOLOv8 displaying the highest performance metrics - Precision of 0.933, Recall of 0.923, mAP50 of 0.956, and mAP50-95 of 0.674 (YOLOv8m exhibits better results than YOLOv10n as the nano version is parametrically smaller and chosen over the bulkier medium version due to computational load). These results represent a substantial improvement over those in Table III, with a **5.1860%** increase in Precision, a **14.8009%** increase in Recall, a **9.5074%** increase in mAP50 and a **19.5035%** increase in mAP50-95 for YOLOv8. Average increases of, **7.6892%** in Precision, **19.9069%** in Recall, **15.8506%** in mAP50 and **23.8099%** in mAP50-95 are observed across all models. The average increase across all metrics is observed to be **16.81%** This

increase in metrics validates our methodology of introducing FDA to curb the effect of adverse weather, pointing to a solution applicable to real-world scenarios.

TABLE III
COMPARISONS OF DIFFERENT MODELS WHEN TRAINED ON D^s (CLEAN)
DATA BUT INFERRRED ON THE D^t (FOGGY AND RAINY) DATA

Model	Class	Precision	Recall	mAP50	mAP50-95
YOLOv10n	All	0.86	0.691	0.774	0.46
	Red	0.891	0.724	0.821	0.53
	Green	0.873	0.651	0.745	0.445
	Yellow	0.815	0.698	0.755	0.405
YOLOv8m	All	0.887	0.804	0.873	0.564
	Red	0.937	0.825	0.91	0.641
	Green	0.886	0.76	0.851	0.553
	Yellow	0.839	0.828	0.859	0.499
YOLOv6m	All	0.82	0.757	0.809	0.52
	Red	0.914	0.793	0.877	0.61
	Green	0.875	0.719	0.819	0.529
	Yellow	0.671	0.758	0.729	0.422
YOLOv5m	All	0.856	0.682	0.766	0.481
	Red	0.915	0.687	0.8147	0.549
	Green	0.87	0.658	0.76	0.484
	Yellow	0.784	0.7	0.722	0.41

As shown in Table III, models trained on D^s and inferred on D^t exhibit sub-par performances. This degradation in metrics highlights how our exhaustive experimentation ensures the addition of not only effective but also realistic rain and fog. It simulates real-world weather conditions in the labelless target domain dataset, thereby validating the observed performance drop and pointing to its real-world applications, where accessing labels.

As demonstrated in Table VI, the class imbalance has been mitigated by incorporating augmented images. The models exhibit excellent performance, especially in detecting yellow lights across various degrees of FDA, as indicated by the parameter β , demonstrating the effectiveness of our methodology. For the value of $\beta=0.15$, we observe an 11.4086% increase in mAP50 and a 20.8416% increase in mAP50-95 for the yellow class in the case of YOLOv8. Similarly, a 25.3772% increase in mAP50 and a 19.9052% increase in mAP50-95 is noted for YOLOv6, and an increase of 29.2243% in mAP50

and 34.3902% in mAP50-95 in the case of YOLOv5.

The effect of our proposed methodology is also evident through the qualitative results, as observed in Fig. 6. Looking closely, it is noted that models tend to detect traffic lights more accurately and with a much higher confidence score. Furthermore, on observing Fig. 7, it is noted through the Negative Samples (NS1, NS2) and Positive Samples (PS1, PS2) that the effect of FDA-augmented images extends to real-world scenarios where training on clean images (D^s) may result in the traffic light not being detected. As evident in the figure, training on FDA-augmented images solves this and results in such traffic lights being properly detected with accurate bounding boxes. This exemplifies the applicability of our methodology in real-world scenarios. In cases with insufficient data on traffic scenes in challenging weather conditions, FDA can be applied to existing data in clear environments. This can help the models generalize and perform better in unforeseen weather conditions. The images in the figure have been obtained by training YOLOv8m on the Clean Dataset (D^s) and the FDA-augmented train set ($D^{s \rightarrow t}$).

Directing our attention to SSL (Table V), it is noted that training on only 50% of the real ground truth labels and generating pseudo labels by employing YOLOv6 for the rest demonstrates comparable results. It is also noted that these results were obtained by training all models that were used for supervised learning, namely, YOLOv5, YOLOv6, YOLOv8, and YOLOv10 on the NVIDIA A6000 for 20 epochs. Although these results might be considered slightly subpar, it is crucial to note that the implementation of SSL in this domain could be influential in leveraging the already scarce data to obtain better results in the future.

VI. CONCLUSION

In this paper, we introduce TLDR, an innovative approach to tackle problems in the domain of Traffic Light Detection under Bad Weather conditions. We address the lack of datasets in this field by compiling two widely used standard Traffic Light Detection datasets. Further, we resolve the severe class imbalance by adding augmentations, then employ pre-existing rain and fog generation techniques to create a realistic dataset. Furthermore, we integrate Fourier Domain Adaptation (FDA).

TABLE IV

RESULTS OF VARIOUS MODELS WHEN TRAINED ON FDA-AUGMENTED DATA AND INFERRED ON D^t . ALL METRICS ARE AVERAGED ACROSS THE 3 CLASSES.

Model	Beta(β)	Precision	Recall	mAP50	mAP50-95
YOLOv10n	0.15	0.911	0.85	0.927	0.617
	0.1	0.903	0.83	0.903	0.58
	0.05	0.935	0.923	0.964	0.682
YOLOv8m	0.15	0.933	0.923	0.956	0.674
	0.1	0.927	0.877	0.927	0.633
	0.05	0.882	0.693	0.767	0.495
YOLOv6m	0.15	0.914	0.856	0.914	0.585
	0.1	0.890	0.772	0.843	0.516
	0.05	0.932	0.919	0.954	0.654
YOLOv5m	0.15	0.926	0.878	0.928	0.621
	0.1	0.887	0.765	0.826	0.532
	0.05	0.850	0.646	0.724	0.439

TABLE V
COMPARISONS OF RESULTS OF VARIOUS MODELS TRAINED USING SSL.
AS MENTIONED IN THE BENCHMARKING AND RESULTS SECTION,
PSEUDOLABELS ARE GENERATED FOR 50% OF THE DATASET USING
YOLOv6M, WHILE THE REST ARE ORIGINAL LABELS.

Model	Class	Precision	Recall	mAP50	mAP50-95
YOLOv10n	All	0.82	0.772	0.838	0.47
	Red	0.816	0.832	0.876	0.54
	Green	0.786	0.718	0.805	0.455
	Yellow	0.86	0.766	0.835	0.414
YOLOv8m	All	0.849	0.826	0.878	0.501
	Red	0.842	0.876	0.908	0.565
	Green	0.808	0.771	0.833	0.478
	Yellow	0.898	0.832	0.892	0.46
YOLOv6m	All	0.82	0.807	0.843	0.472
	Red	0.861	0.862	0.89	0.543
	Green	0.79	0.751	0.81	0.455
	Yellow	0.808	0.808	0.828	0.417
YOLOv5m	All	0.838	0.796	0.85	0.47
	Red	0.828	0.854	0.887	0.532
	Green	0.795	0.745	0.8	0.441
	Yellow	0.892	0.791	0.862	0.438

with our methodology to demonstrate its strengths in detection by showing results by benchmarking various diverse models. Additionally, to counter the lack of datasets, we also explore Semi-supervised Learning, where we train with only 50% of the labels and then demonstrate comparable results. By benchmarking several models, we quantitatively and qualitatively validate the results of FDA and Semi-Supervised Learning (SSL) in the domain of traffic light detection and recognition.

We are currently exploring future work in manipulating images by adding more effects, such as Gaussian Noise or Snow, while also trying to extend our work to detect other traffic signs. Furthermore, we believe that an approach like TLDR can be applied to detecting traffic signs and not just traffic lights. Additionally, we encourage other researchers in this field to create datasets for this purpose in order to make ADAS systems more robust.

REFERENCES

- [1] R. Xu, H. Xiang, X. Xia, X. Han, J. Li, and J. Ma, “Opv2v: An open benchmark dataset and fusion pipeline for perception with vehicle-to-vehicle communication,” in *2022 International Conference on Robotics and Automation (ICRA)*, pp. 2583–2589, 2022.
- [2] X. Zhao, P. Sun, Z. Xu, H. Min, and H. Yu, “Fusion of 3d lidar and camera data for object detection in autonomous vehicle applications,” *IEEE Sensors Journal*, vol. 20, no. 9, pp. 4901–4913, 2020.
- [3] Y. Qiu, Y. Lu, Y. Wang, and H. Jiang, “Idod-yolov7: Image-dehazing yolov7 for object detection in low-light foggy traffic environments,” *Sensors*, vol. 23, no. 3, p. 1347, 2023.
- [4] G. Wang, J. Guo, Y. Chen, Y. Li, and Q. Xu, “A pso and bfo-based learning strategy applied to faster r-cnn for object detection in autonomous driving,” *IEEE Access*, vol. 7, pp. 18840–18859, 2019.
- [5] S. Zang, M. Ding, D. Smith, P. Tyler, T. Rakotoarivelo, and M. A. Kaafar, “The impact of adverse weather conditions on autonomous vehicles: How rain, snow, fog, and hail affect the performance of a self-driving car,” *IEEE vehicular technology magazine*, vol. 14, no. 2, pp. 103–111, 2019.
- [6] M. Bijelic, T. Gruber, F. Mannan, F. Kraus, W. Ritter, K. Dietmayer, and F. Heide, “Seeing through fog without seeing fog: Deep multimodal sensor fusion in unseen adverse weather,” in *Proceedings of the IEEE/CVF Conference on Computer Vision and Pattern Recognition (CVPR)*, June 2020.
- [7] G. Jocher, “Ultralytics yolov5,” 2020.

TABLE VI

CLASS-WISE RESULTS WHEN TRAINED ON THE FDA DATASET AND INFERRED ON THE D^t DATASET. AS EVIDENT ACROSS ALL METRICS, THE QUANTITATIVE RESULTS OF DIFFERENT MODELS ARE IMPRESSIVE, ESPECIALLY FOR THE YELLOW IMAGES, SHOWCASING THE EFFECTIVENESS OF COUNTERING CLASS IMBALANCE.

Model	Beta(β)	Class	Precision	Recall	mAP50	mAP50-95
YOLOv10n	0.15	Red	0.938	0.893	0.952	0.698
		Green	0.912	0.809	0.91	0.623
		Yellow	0.882	0.847	0.918	0.529
	0.1	Red	0.942	0.871	0.94	0.669
		Green	0.895	0.802	0.887	0.586
		Yellow	0.874	0.817	0.883	0.485
	0.05	Red	0.949	0.941	0.973	0.749
		Green	0.922	0.898	0.952	0.687
		Yellow	0.934	0.931	0.966	0.609
YOLOv8m	0.15	Red	0.945	0.942	0.97	0.741
		Green	0.922	0.888	0.942	0.678
		Yellow	0.934	0.939	0.957	0.603
	0.1	Red	0.949	0.899	0.952	0.704
		Green	0.915	0.835	0.9	0.629
		Yellow	0.919	0.898	0.929	0.565
	0.05	Red	0.908	0.71	0.811	0.563
		Green	0.856	0.664	0.738	0.491
		Yellow	0.883	0.703	0.751	0.431
YOLOv6m	0.15	Red	0.934	0.89	0.934	0.662
		Green	0.899	0.813	0.895	0.588
		Yellow	0.908	0.865	0.914	0.506
	0.1	Red	0.932	0.817	0.89	0.599
		Green	0.878	0.732	0.82	0.519
		Yellow	0.859	0.769	0.818	0.432
	0.05	Red	0.952	0.936	0.968	0.730
		Green	0.913	0.895	0.94	0.658
		Yellow	0.931	0.926	0.953	0.574
YOLOv5m	0.15	Red	0.940	0.898	0.950	0.697
		Green	0.909	0.839	0.902	0.615
		Yellow	0.930	0.897	0.933	0.551
	0.1	Red	0.912	0.785	0.867	0.614
		Green	0.849	0.725	0.779	0.516
		Yellow	0.901	0.704	0.832	0.466
	0.05	Red	0.889	0.669	0.78	0.52
		Green	0.804	0.62	0.689	0.437
		Yellow	0.857	0.648	0.703	0.361

[8] C. Li, L. Li, Y. Geng, H. Jiang, M. Cheng, B. Zhang, Z. Ke, X. Xu, and X. Chu, “Yolov6 v3.0: A full-scale reloading,” 2023.

[9] G. Jocher, A. Chaurasia, and J. Qiu, “Ultralytics yolov8,” 2023.

[10] A. Wang, H. Chen, L. Liu, K. Chen, Z. Lin, J. Han, and G. Ding, “Yolov10: Real-time end-to-end object detection,” 2024.

[11] Y. Yang and S. Soatto, “Fda: Fourier domain adaptation for semantic segmentation,” in *Proceedings of the IEEE/CVF conference on computer vision and pattern recognition*, pp. 4085–4095, 2020.

[12] M. B. Jensen, M. P. Philipsen, A. Møgelmose, T. B. Moeslund, and M. M. Trivedi, “Vision for looking at traffic lights: Issues, survey, and perspectives,” *IEEE Transactions on Intelligent Transportation Systems*, vol. 17, no. 7, pp. 1800–1815, 2016.

[13] X. Yang, J. Yan, W. Liao, X. Yang, J. Tang, and T. He, “Scrdet++: Detecting small, cluttered and rotated objects via instance-level feature denoising and rotation loss smoothing,” *IEEE Transactions on Pattern Analysis and Machine Intelligence*, 2022.

[14] L.-A. Tran, C. N. Tran, D.-C. Park, J. Carrabina, and D. Castells-Rufas, “Toward improving robustness of object detectors against domain shift,” in *2024 International Conference on Green Energy, Computing and Sustainable Technology (GECOST)*, pp. 01–05, IEEE, 2024.

[15] J. Redmon and A. Farhadi, “Yolov3: An incremental improvement,” *arXiv preprint arXiv:1804.02767*, 2018.

[16] K. He, G. Gkioxari, P. Dollár, and R. Girshick, “Mask r-cnn,” in *Proceedings of the IEEE international conference on computer vision*, pp. 2961–2969, 2017.

[17] N. Carion, F. Massa, G. Synnaeve, N. Usunier, A. Kirillov, and S. Zagoruyko, “End-to-end object detection with transformers,” 2020.

[18] T. Sharma, B. Debaque, N. Duclos, A. Chehri, B. Kinder, and P. Fortier, “Deep learning-based object detection and scene perception under bad weather conditions,” *Electronics*, vol. 11, no. 4, 2022.

[19] Y. Han and D. Hu, “Multispectral fusion approach for traffic target detection in bad weather,” *Algorithms*, vol. 13, no. 11, 2020.

[20] J. Kim, H. Cho, M. Hwangbo, J. Choi, J. Canny, and Y. P. Kwon, “Deep traffic light detection for self-driving cars from a large-scale dataset,” in *2018 21st International Conference on Intelligent Transportation Systems (ITSC)*, pp. 280–285, 2018.

[21] P. M. Nguyen, V. C. Nguyen, S. N. Nguyen, L. M. T. Dang, H. X. Nguyen, and V. D. Nguyen, “Robust traffic light detection and classification under day and night conditions,” in *2020 20th International Conference on Control, Automation and Systems (ICCAS)*, pp. 565–570, 2020.

[22] Y. Zhao, Y. Feng, Y. Wang, Z. Zhang, and Z. Zhang, “Study on detection and recognition of traffic lights based on improved yolov4,” *Sensors*, vol. 22, no. 20, 2022.

[23] L. Gou, L. Zou, N. Li, M. Hofmann, A. K. Shekar, A. Wendt, and L. Ren, “Vatld: A visual analytics system to assess, understand and improve traffic light detection,” 2020.

[24] E. Tzeng, J. Hoffman, K. Saenko, and T. Darrell, “Adversarial discriminative domain adaptation,” in *Proceedings of the IEEE Conference on Computer Vision and Pattern Recognition (CVPR)*, July 2017.

[25] M. Long, Y. Cao, Z. Cao, J. Wang, and M. I. Jordan, “Transferable representation learning with deep adaptation networks,” *IEEE Transactions on Pattern Analysis and Machine Intelligence*, vol. 41, no. 12, pp. 3071–3085, 2019.

- [26] Y. Yang and S. Soatto, "Fda: Fourier domain adaptation for semantic segmentation," in *Proceedings of the IEEE/CVF Conference on Computer Vision and Pattern Recognition (CVPR)*, June 2020.
- [27] J. Wang, Q. Wu, T. Liu, Y. Wang, P. Li, T. Yuan, and Z. Ji, "Fourier domain adaptation for the identification of grape leaf diseases," *Applied Sciences*, vol. 14, no. 9, 2024.
- [28] J. Li, H. Gang, H. Ma, M. Tomizuka, and C. Choi, "Important object identification with semi-supervised learning for autonomous driving," in *2022 International Conference on Robotics and Automation (ICRA)*, pp. 2913–2919, 2022.
- [29] T. Liu, Y. Yang, G.-B. Huang, Y. K. Yeo, and Z. Lin, "Driver distraction detection using semi-supervised machine learning," *IEEE Transactions on Intelligent Transportation Systems*, vol. 17, no. 4, pp. 1108–1120, 2016.
- [30] A. Buslaev, V. I. Iglovikov, E. Khvedchenya, A. Parinov, M. Druzhinin, and A. A. Kalinin, "Albumentations: fast and flexible image augmentations," *Information*, vol. 11, no. 2, p. 125, 2020.
- [31] M. Frigo and S. G. Johnson, "Fftw: An adaptive software architecture for the fft," in *Proceedings of the 1998 IEEE International Conference on Acoustics, Speech and Signal Processing, ICASSP'98 (Cat. No. 98CH36181)*, vol. 3, pp. 1381–1384, IEEE, 1998.
- [32] K. Weng, X. Chu, X. Xu, J. Huang, and X. Wei, "Efficientrep: An efficient repvgg-style convnets with hardware-aware neural network design," *arXiv preprint arXiv:2302.00386*, 2023.
- [33] X. Ding, X. Zhang, N. Ma, J. Han, G. Ding, and J. Sun, "Repvgg: Making vgg-style convnets great again," 2021.
- [34] D. P. Kingma and J. Ba, "Adam: A method for stochastic optimization," 2017.
- [35] J. Redmon, S. Divvala, R. Girshick, and A. Farhadi, "You only look once: Unified, real-time object detection," 2016.
- [36] R. Girshick, J. Donahue, T. Darrell, and J. Malik, "Rich feature hierarchies for accurate object detection and semantic segmentation," 2014.